



## Rigorous steady state modeling of MSF–BR desalination system

Fuad N. Alasfour\*, Hassan K. Abdulrahim

*Kuwait University, College of Engineering and Petroleum, Mechanical Engineering Department, P.O. Box 5969 Safat 13060, Kuwait  
Tel. +965 481-1188 ext. 5799; Fax +965 484-7131; email: alasfour@kuc01.kuniv.edu.kw, ahassan@kuc01.kuniv.edu.kw*

Received 29 August 2007; accepted revised 10 August 2008

---

### ABSTRACT

The aim of this paper is to model and simulate a multistage flashing with brine recirculation (MSF–BR) desalination system. A rigorous steady state mathematical model was formulated and implemented using process simulation software IPSEpro®. To enable detailed simulation of the processes, the flashing stage was decomposed into three main components; flashing pool, distillate tray and tube bundle. The model considered thermo-physical properties as a function of temperature and salinity, in addition, the stream enthalpy was used in the model instead of the specific heat to account for the effect of infinitesimal changes in temperature. The energy losses from the flashing stage and the brine heater were taken into consideration. The overall heat transfer coefficient was evaluated at each stage using convective heat transfer coefficient for internal and external flows, beside thermal and fouling resistance. The variation in tube thermal conductivity with temperature was also considered in the heat transfer analysis. The developed model was used to predict the performance of MSF–BR processes in the light of first and second law of thermodynamics. The computational results obtained in this research were verified and validated against the actual data at MSF–BR Azzour South Plant in Kuwait. Results showed good agreement between the computational results and actual plant data.

*Keywords:* MSF–BR; Steady state; Modeling; First and second law; Desalination

---

### 1. Introduction

Supplying fresh water is one of the main concerns in countries with scarce and limited fresh water resources. In the Gulf countries, people depend mainly on desalted water to satisfy their needs of potable water, large quantities of desalted water are produced using MSF desalting plants with capacities up to 16 MIGD, the most common used type in Kuwait is MSF; it is the most mature and reliable desalination system since 1960's. In the last three decades, a tremendous effort was concentrated on MSF system to reduce the specific energy consumption where several researchers implemented rigorous predictive mathematical models to understand desalination

processes in order to enhance the performance of MSF system.

In literature, several MSF mathematical models have been developed and tested, a great deal of studies are aimed to develop a simple and efficient mathematical model that can predict real MSF performance. These models can be classified into steady state and dynamic models. Steady state models are the most used ones during the plant design phase and for existing plant reassessment [1–3], whereas dynamic models are usually used for designing control system and checking plant operation stability [4–6].

### 2. Literature review

Steady state mathematical models are usually utilized

---

\* Corresponding author.

during plant design and operation evaluation; these models are well established and developed using the basic laws of thermodynamics. Models can range from simple steady state models with constant stream thermo-physical properties [1–3] to rigorous models which consider properties variations and losses [4,5].

Soliman [1] developed a steady state mathematical model for MSF–BR, he considered different operating parameters for each plant section. The model was very fast in convergence and suitable for optimization. The following assumptions were considered:

1. Constant value of specific heat, temperature difference per stage, heat transfer coefficient and heat transfer area.
2. Constant value of boiling point elevation losses.
3. Neglecting the non-equilibrium allowance.

The model was used to investigate the effect of varying cooling water temperature and/or flow rate on plant performance, at constant distillate production or constant steam consumption, his results showed a good agreement with other complex models [2].

Helal [3] and Helal et al. [7] developed a mathematical model to study the feasibility of upgrading an existing MSF–BR plant. The model used SOLVER optimization tool of Microsoft Excel® software to maximize plant capacity. Several constraints were imposed to ensure that the plant can operate satisfactory at the suggested operating conditions. These constraints were:

1. Maximum flow rate of recycled brine, intake, distillate, blow down and steam are limited by the maximum capacity of the respective pumps.
2. Brine velocity in the condenser pipes is in the range of 1.5–2.3 m/s.
3. Maximum top brine temperature (110°C) is limited by the available steam temperature and anti-scalant type.
4. Maximum blow down concentration is 80,000 ppm.

The model was applied on Umm Al-Nar East MSF–BR plant. The optimized results obtained were verified against the counterparts with good agreement.

The other category of MSF models are rigorous models, where the effect of temperature and salinity on the stream thermo-physical properties are considered. The stage temperature difference is calculated from the stage energy balance with non linear temperature profiles. In addition, heat transfer coefficient is calculated at each stage, while temperature losses and pressure drop are considered.

Helal et al. [8] developed an efficient and reliable technique to solve a detailed MSF model. The proposed technique formulated the model equations in a tri-diagonal matrix (TDM) form, via: (a) linearization of the non-linear equations and (b) decomposes the equations into subsets grouped by type rather than by stage. The TDM

was solved using Thomas algorithm. The model considered several thermodynamic losses such as non-equilibrium allowance, boiling point elevation and temperature losses due to the drop in pressure across the demister and condenser tube bundle. A computer program was developed based on the proposed model and showed very fast and stable convergence over a wide range of operating conditions. The developed program was capable to simulate both MSF–BR and MSF–OT systems. The assumptions used by the authors were: salt free product, adiabatic processes, neglecting heat of mixing brine solution, and no sub cooling of condensate leaving the brine heater.

The model also considered the variation of thermo-physical properties of the brine as a function of temperature and salinity. A simplified model was solved to produce a good initial guess for the detailed model which improved the convergence speed of the detailed model. The results were verified against actual data at Al-Khobar II MSF plant and showed a good agreement. One of the advantages of the developed TDM algorithm was its minimum loop nesting and high convergence stability and reliability. Although the algorithm was very efficient and ensured rapid convergence, the linearization process was very complicated, not straightforward and required many mathematical manipulation steps.

Al-Mutaz et al. [9] proposed a steady state simulation method for MSF systems. In their model, very few stages were solved instead of solving mass and energy balance for all stages. The application of the new method showed that it is remarkably efficient and at least twice faster than the method based on simultaneous solution for all stages. The proposed method was used to simulate an existing MSF plant at Al-Khobar II, and results showed good agreement. The results of the proposed method were also compared against the TDM method used by Helal et al. [8] and showed very good agreement. The proposed method needs less computational time compared to the TDM method.

Husain et al. [10] presented a mathematical model for simulation, optimization and control of MSF–BR plants. In their study, the authors divided the flashing stage into four components: brine pool, product tray, vapor space and tube bundle. Through their rigorous model they balance mass flow, salt content and flow enthalpy were for each component, in addition they considered heat transfer between tube bundle and vapor space. The model was supported by correlations for brine densities, boiling temperatures, brine and vapor enthalpies and heat transfer coefficients, temperature losses due to boiling point elevation; non-equilibrium allowance and pressure losses in demister were included in the model. The authors explained the main sources of inaccuracies in their mathematical model, where these sources were: heat transfer coefficient correlations and non-equilibrium allowance where the predicted heat transfer coefficient

using analytical correlations differed by 10% from the actual data; the differences were due to the presence of non-condensable gases and accumulation of fouling on heat transfer surfaces. With fixing the system degree of freedom, the model was solved using TDM technique and a commercial software SpeedUp. Also specially designed FORTRAN code was developed based on TDM algorithm to solve the model. The results were compared between TDM using FORTRAN code and SpeedUp software; their results showed a large difference in the temperature profile between the design data and the predicted ones, it reached 13% in the cooling brine temperature in the first stage, and with minimum error of 5% at low temperature side of the plant. When an arbitrary fouling factor was introduced, the maximum error was reduced to 12.5%. SpeedUp software showed better performance than the TDM using FORTRAN code.

Aly et al. [11] suggested a model which considered the conservation of mass and energy in all MSF–BR sections, with supplementary correlations for heat transfer and thermo-physical properties. The authors used their model to simulate an existing desalination plant at Al-Khobar-II, in order to investigate the possibility of increasing plant production rate and keep cost minimum. They investigated the performance of the plant under different operating conditions. The model was used to test the plant performance over an extended TBT range from 88 to 115°C and seawater temperature from 10 to 40°C. The TDM technique was used in their model. Results showed that uprating is a promising technique for increasing the production rate through elevated values of TBT. However, the only concern was fouling and scale formation.

El-Dessouky et al. [12] developed a steady state mathematical model to analyze an MSF–BR system. The developed model was suitable for either design of a new plant or for evaluation of the performance of an existing plant under different operating conditions. The variation of thermo-physical properties of seawater with temperature and salt concentration was considered. The model considered flashing of the accumulated condensate in the distillate tray due to the pressure drop from one stage to another. The fouling resistance effect on heat transfer area was also considered in the calculation of the overall heat transfer coefficient, where constant fouling resistance value was used in each plant section. The effect of the non-condensable gases on the overall heat transfer coefficient was neglected in their model. The model results were verified against actual data at Doha West plant and showed a good agreement. The energy balance equations were based on specific heat and stage temperature difference. The authors assumed constant specific heat which evaluated at average plant temperature. The model solution was an iterative type and depended on the initial values assigned to the variables.

El-Dessouky et al. [13,14] presented a stage-to-stage

algorithm for solving equations describing the steady state behavior of an MSF plant. The proposed algorithm decompose equations describing MSF processes into three groups and solved them using a reliable and efficient one dimensional fixed point iteration method. The main advantages of the proposed algorithm were: (1) less sensitive to initial guess, (2) fewer iteration steps to obtain the required solution and (3) no derivative calculations were required. The model was used to predict the temperature profile and distillate in each stage. The results were verified against actual data at Doha West plant. Results showed good agreement against the plant data.

Thomas et al. [15] developed a mathematical model to simulate both steady and dynamic behavior of the MSF–BR system. The steady and dynamic models were based on the same set of equations. They used steady state model to predict the effect of the operating parameters on the system performance; while the dynamic model was useful for designing the system controllers and optimizing parameters. The flashing stage was divided into four control volumes: flashing brine tray, distillate tray, vapor space and condenser tubes. The model accounted for the temperature losses due to boiling point elevation, non-equilibrium allowance, and pressure losses in the demister and tube bundle. Results were compared against real operating data at unit five of Umm Al-Nar East Extension. The predicted temperatures of the flashing brine and vapor showed an excellent agreement. Other principle operating parameters such as distillate flow rate, blow down TDS were also predicted excellently. However, the predicted condensate flow rate from the brine heater was higher than the actual plant data, and hence lower performance ratio was obtained assuming high fouling factor.

Aly et al. [16] developed a steady state mathematical model to analyze an MSF plant. The model accounted for the geometry of the stages, the mechanism of heat transfer and the variation of the thermo-physical properties of brine with temperature and salinity. In addition, the model took into consideration the role of fouling and its effect on plant performance ratio. Model assumptions were: constant specific heat, adiabatic processes, and salt free distillate. They neglected the flashing process from the distillate tray and assumed no sub-cooling for the condensate. On the other hand, they included the effect of boiling point elevation, non-equilibrium allowance and temperature losses in the demister and tube bundle for flashed vapor temperature calculation. The authors used semi-empirical formulas for heat transfer coefficient and assumed constant value for fouling resistance of 0.0001205 and 0.00018 m<sup>2</sup> °C/W for heat recovery and heat rejection sections, respectively. The calculation of heat transfer coefficient was based on the equation developed by Griffin et al. [2], which was used by several researchers [1,8,17]. The model was able to predict different temperature profiles and mass flow rate

at each stage, and evaluated the effect of operation parameters such as TBT, seawater temperature and recirculation flow rate on the plant performance. Their results were verified against actual data at Sidi-Krir plant, results showed a good agreement between model output and plant vendor data.

Table 1 shows a comparison between the assumptions of a conventional model(s) and the suggested model.

The aim of this research is to develop a rigorous steady state mathematical model for MSF–BR desalination system. A process simulator software IPSEpro® will be used to simulate the system. The results will be checked and verified against actual data at Azzour South desalination plant. In the light of first and second laws, the model will be used to predict the performance of MSF–BR system.

### 3. Mathematical model

In this research, the proposed MSF–BR model considers the dependence of thermo-physical properties on both temperature and salinity. The streams enthalpy was used in the energy analysis instead of specific heat to account for the effect of infinitesimal changes of temperature. In addition, the energy losses from the flashing stage and the brine heater to the environment were taken into consideration. The overall heat transfer coefficient was evaluated at each stage using convective heat transfer coefficient formulas for internal and external flows, thermal resistance of tube material, and fouling resistance

on outer and inner tube surfaces. The variation of thermal conductivity of tube material with tube temperature was also considered in the heat transfer analysis. Different types of losses due to boiling point elevations, non-equilibrium allowance, and temperature losses due to pressure losses in the demister and tube bundle been considered in this model. In this analysis, the MSF–BR stage was decomposed into three basic components; flashing pool, distillate tray, and tube bundle.

Fig. 1 presents a schematic diagram of flashing stage basic components. The following principals were considered during the development of the present model:

1. No predefined temperature profile assumption for any stream.
2. Flashing brine temperature drop ( $\Delta T$ ) and recirculation brine temperature rise ( $\Delta t$ ) across stages are neither constant nor equal.
3. Thermo-physical properties of saline water are function of both temperature and salinity, while for vapor and distillate are function of temperature only.
4. Since heat transfer in flashing stage is a complicated process, hence heat transfer coefficient and heat transfer area are evaluated using the most accurate procedure available in the literature.
5. Flashing stages and brine heater are not adiabatic, and heat losses to environment are accounted.

#### 3.1. Flashing pool model

Fig. 2 shows the schematic diagram of the flashing pool, the mass and heat balances are given by:

Table 1  
Comparison between the assumptions of a conventional model(s) and the suggested model

Conventional model assumptions	Suggested model assumptions
Constant temperature drop across the stage.	The model will calculate the actual temperature drop of each stage.
Constant specific heat for brine and distillate.	The enthalpy of each stream as function of both temperature and/or salinity is used instead of specific heat.
Constant heat transfer coefficient.	Heat transfer coefficient is evaluated using analytical correlations for each stage.
Neglected heat loss to the surroundings.	Heat loss to the surrounding is accounted for by using thermal efficiency for each component in the stage.
The non-condensable gases have negligible effect on the heat transfer process.	The effect of non-condensable gases on heat transfer coefficient is considered.
Effects of boiling point elevation and non-equilibrium losses on the stage energy balance are negligible; however, their effects are included in the design of the condenser heat transfer area.	Boiling point elevation, non-equilibrium allowance, demister and tube bundle temperature losses are included in this model and been evaluated for each stage. Their effects on both stage energy balance and heat transfer coefficient are also considered.
Heat and mass losses to the vacuum system are neglected.	Heat and mass losses to the vacuum system are considered.

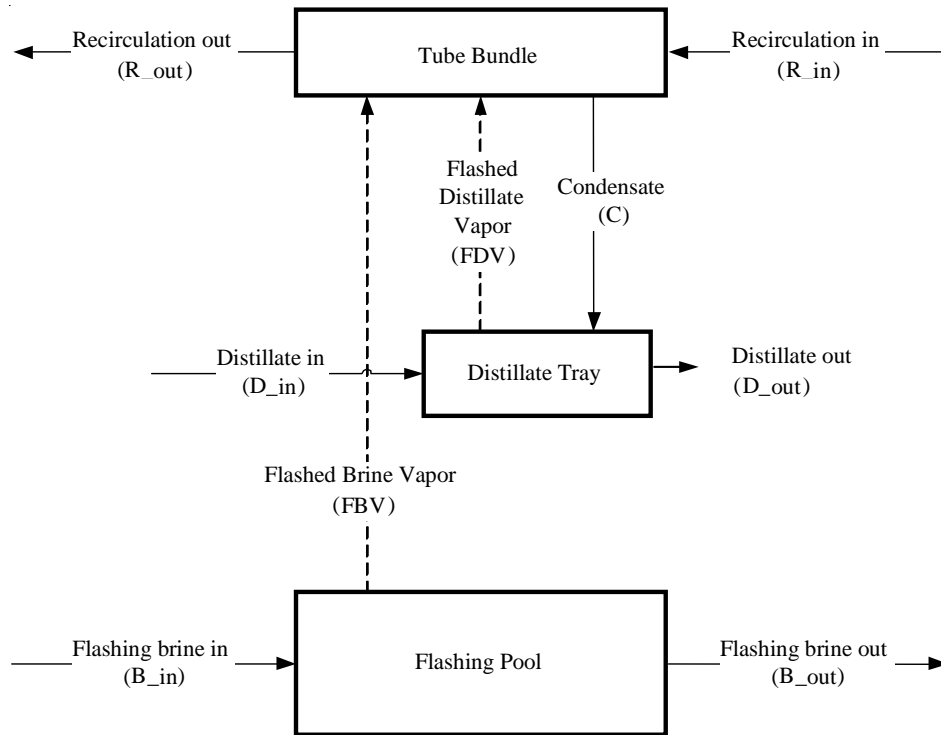


Fig. 1. Flashing stage components.

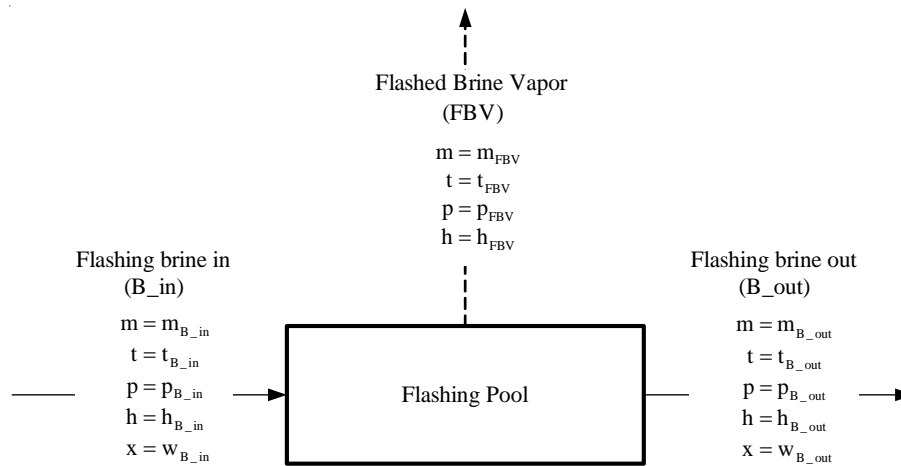


Fig. 2. Schematic diagram for the flashing pool model.

Mass balance

$$m_{B\_in} = m_{B\_out} + m_{FBV} \tag{1}$$

Salt mass balance

$$m_{B\_in} w_{B\_in} = m_{B\_out} w_{B\_out} \tag{2}$$

Energy balance

$$\eta_{FP} (m_{B\_in} h_{B\_in} - m_{B\_out} h_{B\_out}) = m_{FBV} h_{FBV} \tag{3}$$

Temperature drop

$$\Delta T = t_{B\_in} - t_{B\_out} \tag{4}$$

(2) The brine is assumed to leave the flashing pool at saturation condition, and is calculated as a function of temperature and salinity of the exit brine conditions.

(3) The flashed distillate vapor temperature at the condenser surface is calculated using

$$t_{FBV} = t_{B\_out} - \sum \Delta T_{loss} \quad (5)$$

where

$$\sum \Delta T_{loss} = T_{BPE} + T_{NEA} + \Delta T_{dem} + \Delta T_{TB} \quad (6)$$

where  $T_{BPE}$ ,  $T_{NEA}$ ,  $\Delta T_{dem}$  and  $\Delta T_{TB}$  are evaluated using equations provided in Appendix A.

Note that, since the flashing process is not under equilibrium, the pressure of the flashed vapor is equal to the partial pressure of vapor in seawater solution, which is less than the brine pressure.

The exergy destruction in the flashing pool can be expressed as

$$ExD_{FP} = m_{B\_in} e_{B\_in} - m_{B\_out} e_{B\_out} - m_{FBV} e_{FBV} \quad (7)$$

where the stream specific exergy represents the summation of thermal, chemical and pressure exergies of the flowing streams, the detailed calculation is presented in Appendix B.

### 3.2. Distillate tray model

Fig. 3 shows the schematic diagram of distillate tray model. The flashed vapor from distillate tray due to pressure drop is considered in this model. It is worth noting that, the flashed distillate vapor from the distillate tray can flow only over the tube bundle and condensed back to the tray, there is no chance for this vapor to mix with the flashed brine vapor before flowing over the bundle, that is the reason why vapor space been omitted from the model.

Mass balance

$$m_{D\_out} + m_{FDV} = m_{D\_in} + m_{C\_in} \quad (8)$$

Energy balance

$$m_{D\_out} h_{D\_out} + m_{FDV} h_{FDV} = m_{D\_in} h_{D\_in} + m_C h_C \quad (9)$$

Temperature drop

$$\Delta T = t_{D\_in} - t_{D\_out} \quad (10)$$

In this analysis, the distillate temperature drop is equal to the flashing brine temperature drop since both streams experienced the same pressure drop. The non-equilibrium allowance in the distillate tray was ignored in this model, since the distillate tray is shallow and the amount of distillate flow is small compared to the flashing brine flow, And the distillate exits from the distillate tray is considered as saturated liquid at the distillate temperature, while the flashed distillate vapor is assumed as saturated vapor at the distillate tray pressure.

The exergy destruction in the distillate tray can be expressed as

$$ExD_{DT} = m_{D\_in} e_{D\_in} + m_C e_C - m_{D\_out} e_{D\_out} - m_{FDV} e_{FDV} \quad (11)$$

### 3.3. Tube bundle model

Fig. 4 shows a schematic diagram of tube bundle model. The flashed brine vapor and flashed distillate vapor flow over the tube bundle in order to condense, where the condensate flows back to the distillate tray. The effect of pressure loss over the tube bundle on the heat transfer coefficient was neglected in this model. However, the effect of the pressure loss across the tube bundle on the energy balance was considered in the form of temperature drop, as discussed earlier. The condensate was considered as a saturated liquid at a temperature of  $t_C$ . The effect of condensate sub-cooling on the energy balance was evaluated as function of sub-cooling temperature, and the effect of mass loss to the venting system on the energy balance was considered.

Mass balance

$$m_{FBV} + m_{FDV} - m_{vent} = m_C \quad (12)$$

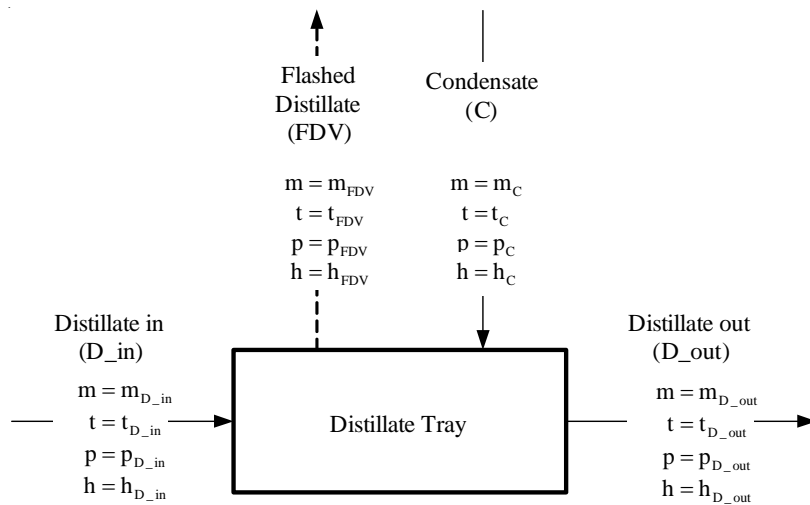


Fig. 3. Distillate tray model.

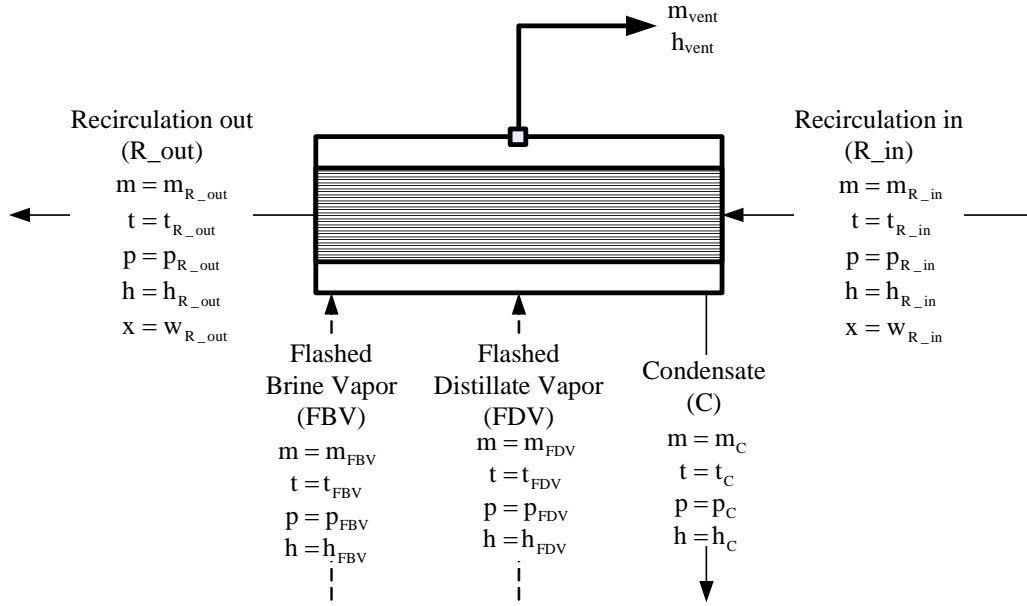


Fig. 4. Tube bundle model.

Energy balance on vapor side

$$Q_{trans} = \eta_{stage} (m_{FDV}h_{FDV} + m_{FBV}h_{FBV} - m_C h_C - m_{vent}h_{vent}) \quad (13)$$

$m_{vent}$  is the mass flow to the venting system and  $h_{vent}$  is equal to vapor enthalpy.

Energy balance for recirculation brine flowing inside the tubes

$$Q_{trans} = m_{R\_out}h_{R\_out} - m_{R\_in}h_{R\_in} \quad (14)$$

$$p_C = p_{FBV} - \Delta P_{vapor} \quad (15)$$

where  $p_C$  is the condensate pressure and  $\Delta P_{vapor}$  is the vapor pressure loss over the tube bundle. The exit recirculation pressure is calculated as following

$$p_{R\_out} = p_{R\_in} - \Delta P_{brine} \quad (16)$$

where  $\Delta P_{brine}$  represents the pressure loss of recirculation brine and is assumed to be constant in this model (0.29 bar). Heat transfer is calculated as

$$Q_{trans} = U_o A_{surface} LMTD \quad (17)$$

where logarithmic mean temperature difference is calculated using

$$LMTD = \frac{\Delta t_{in} - \Delta t_{out}}{\ln\left(\frac{\Delta t_{in}}{\Delta t_{out}}\right)} \quad (18)$$

where

$$\begin{aligned} \Delta t_{in} &= t_C - t_{R\_in} \\ \Delta t_{out} &= t_{FBV} - t_{R\_out} \end{aligned} \quad (19)$$

and heat transfer surface area is

$$A_{surface} = (\pi d_o L_{tube}) N_{tube} \quad (20)$$

The overall heat transfer coefficient based on outer surface area of the tubes is evaluated using [20–22]

$$\frac{1}{U_o} = \left(\frac{d_o}{h_i d_i}\right) + \left(R_{f,i} \frac{d_o}{d_i}\right) + \left(\frac{d_o}{2k_{tube}}\right) \ln\left(\frac{d_o}{d_i}\right) + R_{f,o} + \left(\frac{1}{h_o}\right) \quad (21)$$

The effect of fouling on heat transfer coefficient was considered in this model, the fouling resistance was used on inner and outer tube surfaces  $R_{f,i}$  and  $R_{f,o}$ , respectively. The convective heat transfer coefficients for inner and outer surfaces,  $h_i$  and  $h_o$ , were estimated using empirical correlations [12,13].

The convective heat transfer coefficient for the brine side was calculated using the modified correlation of Dittus and Boelter [23].

$$h_i = 0.027 \left(\frac{k_b}{d_i}\right) Re^{0.8} Pr^{1/3} \left(\frac{\mu_b}{\mu_{b,w}}\right)^{0.14} \quad (22)$$

The thermo-physical properties in Eq. (22) were evaluated at the brine mean bulk temperature except  $\mu_{b,w}$  which been evaluated at wall temperature conditions.

Brine velocity inside tubes was calculated using average brine specific volume between inlet and outlet conditions.

$$V_b = \frac{m_{R\_in}}{A_{cross}} \left(\frac{v_{R\_in} + v_{R\_out}}{2}\right) \quad (23)$$

With tube cross section area for single flow direction

$$A_{\text{cross}} = \left( \frac{\pi}{4} d_i^2 \right) N_{\text{tube}} \quad (24)$$

The condensation heat transfer coefficient for the vapor side is [20]

$$h_o = 0.725 \left( \frac{g k_1^3 \rho_1^2 \lambda_v}{n d_o \mu_1 \delta T} \right)^{0.25} C_1 C_2 \quad (25)$$

where  $\delta T$  is the temperature difference between the condensate and the tube wall temperatures, it is considered as the driving force for the condensation process on the outer surface of the tubes.

$$\delta T = t_c - T_{\text{wall}} \quad (26)$$

The liquid properties in Eq. (25) were evaluated at the film temperature of the tube outer surface. The film temperature  $T_{\text{film}}$  was calculated as

$$T_{\text{film}} = \frac{T_{\text{wall}} + t_c}{2} \quad (27)$$

and the tube wall temperature

$$T_{\text{wall}} = \frac{T_b + t_c}{2} \quad (28)$$

where the average bulk temperature of the recycle brine is

$$T_b = \frac{t_{R\_in} + t_{R\_out}}{2} \quad (29)$$

In Eq. (25),  $C_1$  and  $C_2$  represent the correction factors for the number of tubes in vertical direction and non-condensable gas, respectively.

$$C_1 = 1.23795 + 0.353808 N - 0.0017035 N^2 \quad (30)$$

$$C_2 = 1.0 - 34.313 NCG + 1226.8 NCG^2 - 14923.0 NCG^3 \quad (31)$$

where  $N$  depends on the tube bundle geometry, in the case of rectangular pitch tube bundle the following correlation can be used [23]

$$N = 0.564 \sqrt{N_{\text{tube}}} \quad (32)$$

While in case of equilateral triangular pitch, the following correlation can be used

$$N = 0.481 (N_{\text{tube}})^{0.505} \quad (33)$$

$NCG$  represents the percentage of the non-condensable gases that accumulate in the stage.

The exergy destruction of the tube bundle is calculated as

$$\begin{aligned} ExD_{\text{TB}} = & (m_{R\_in} e_{R\_in} + m_{\text{FBV}} e_{\text{FBV}} + m_{\text{FDV}} e_{\text{FDV}}) \\ & - m_C e_C - m_{R\_out} e_{R\_out} \end{aligned} \quad (34)$$

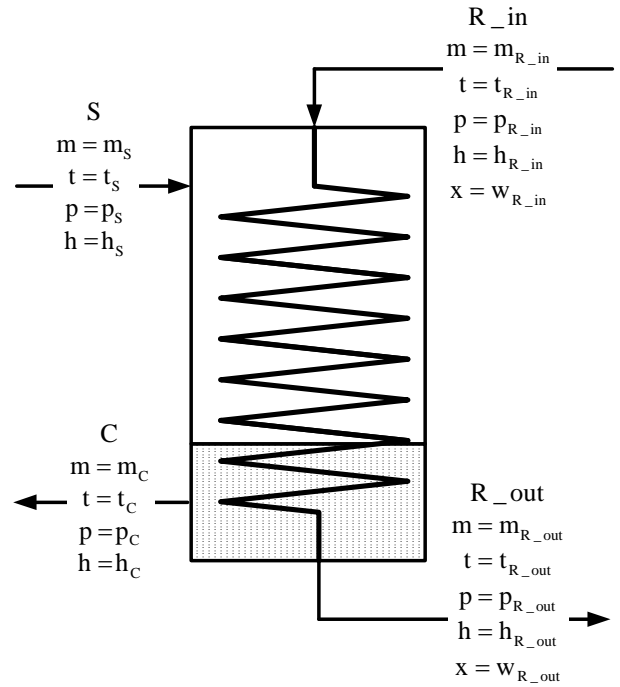


Fig. 5. Brine heater model notations.

### 3.4. Brine heater model

The brine heater represents the heat input section in the MSF system. The model for the brine heater is very similar to that used for the tube bundle. The steam is supplied to the brine heater as saturated vapor and leave as saturated liquid; however, any other steam conditions can be implemented because the model considers the inlet and outlet steam enthalpies. Non-condensable gases do not exist in the brine heater, so that there is no venting from the brine heater. Fig. 5 represents the notations used in the brine heater model.

#### 3.4.1. Thermodynamic model of the brine heater

The mass and energy balances of the brine heater can be estimated using the following equations

Mass balance on steam side

$$m_s = m_c \quad (35)$$

Energy balance on steam side

$$Q_{\text{trans}} = \eta_{\text{BH}} (m_s h_s - m_c h_c) \quad (36)$$

where  $\eta_{\text{BH}}$  is the thermal efficiency of the brine heater, and will be used to account for the heat losses from the brine heater.  $Q_{\text{trans}}$  is the heat transferred from the steam to the recirculation brine inside the tubes. Eqs. (14)–(34) will be used for the brine heater after modifying the notations to brine heater. In Eq. (25)  $C_2 = 1.0$  will be used because there is no gases on the tube surface of the brine heater.

#### 4. Results and discussion

In this research, MSF–BR desalination processes were modeled and simulated in the light of first and second laws of thermodynamics. The developed model was compiled and solved using IPSEpro® software [24,25]. The software description and model solving methodology are explained in details in Abdulrahim [25]. The results were verified against actual data at Azzour South MSF–BR desalination plant in Kuwait. Figs. 5a and 5b show the flow sheet diagrams of MSF–BR process, while Fig. 6 shows the flashing stage details. Fig. 7 shows the pressure and temperature profiles at each flashing stage, results showed that the pressure in each stage is kept less than the pressure in the preceding one to enable the flashing process to continue. One can notice that the pressure in the first stage is at sub-atmospheric due to low top brine temperature used in the calculation. Since, the flashing brine as well as the generated vapor is at saturated condition, hence the temperature profile followed the pressure profile trend; as the pressure decreased the saturation temperatures decreased. Results also showed a very good agreement between model results and the plant actual data. The vapor temperature behaved similar to the brine temperature profile, the difference between the brine temperature and vapor temperature was due to the following stage temperature losses; (i) boiling point elevation, (ii) non-equilibrium allowance, and (iii) temperature losses associated with the pressure losses in demister and tube bundle.

The boiling point elevation and non-equilibrium allowance temperature losses in each stage are depicted in Fig. 8. The predicted results for boiling point elevation showed a good agreement with the actual data. The model prediction for non-equilibrium allowance varies from the actual data especially at the low temperature side of the plant. It is important to mention that several empirical formulas are available in the literature to cal-

culate the non-equilibrium allowance temperature losses, which depend on plant design and operating parameters such as; stage dimension, brine temperature drop and flow rate. In most cases the available empirical formulas are based on experimental results from pilot plants. The generalizations of such formulas to be utilized for other plants at different operating conditions are not recommended in most cases. Results showed that the model gives acceptable results at the high temperature side of the plant.

The flow rates of distillate and brine in each stage are illustrated in Fig. 9. The results show that the increase in distillate flow rate is due to the accumulation of formed distillate from the previous stages. The model was able to predict the flow rate with very good accuracy. Fig. 9 shows that as the distillate flow rate increases the brine flow rate decreases due to the mass conservation. Again, the model prediction and plant actual data were in a good agreement.

The brine salinity profile is shown in Fig. 10. Since distillate is salt free, the results show that the brine salinity increases as the flashing brine flow rate decreases in each stage.

Fig. 11 presents the overall heat transfer coefficient for each stage. The calculated results show a difference from the actual data especially in stages 1–8. The overall heat transfer coefficient depends on the fouling factor and the amount of non-condensable gases among others parameters. The fouling factor was assumed to be constant in each section of the plant: heat input section, heat recovery section and heat rejection section. The non-condensable gas amount was also assumed to be constant in all stages. In real plant, the released gases from the brine due to the flashing process increase the amount of the non-condensable gases in the first stages causing the heat transfer coefficient to be low. The difference between the model prediction and the actual plant data is mainly due to using constant values of the fouling factor and non-

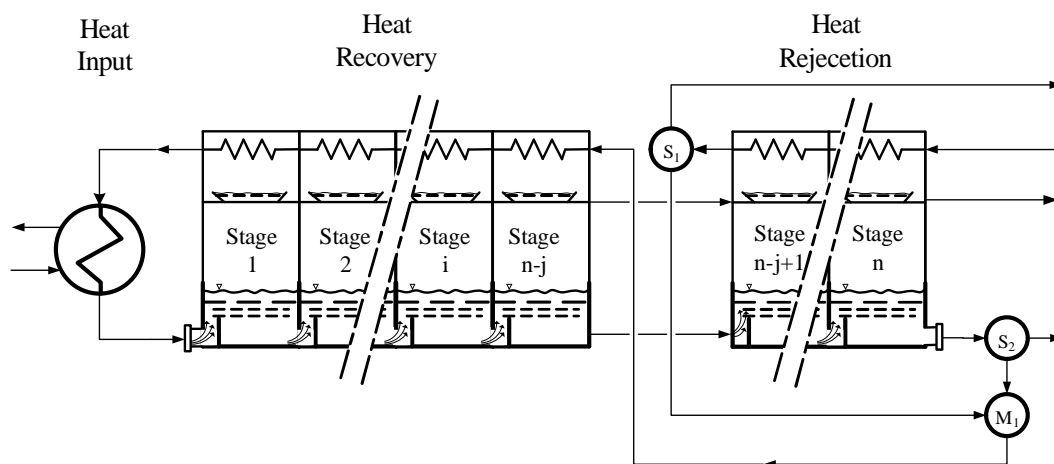


Fig. 5a. Schematic diagram for the MSF–BR system.

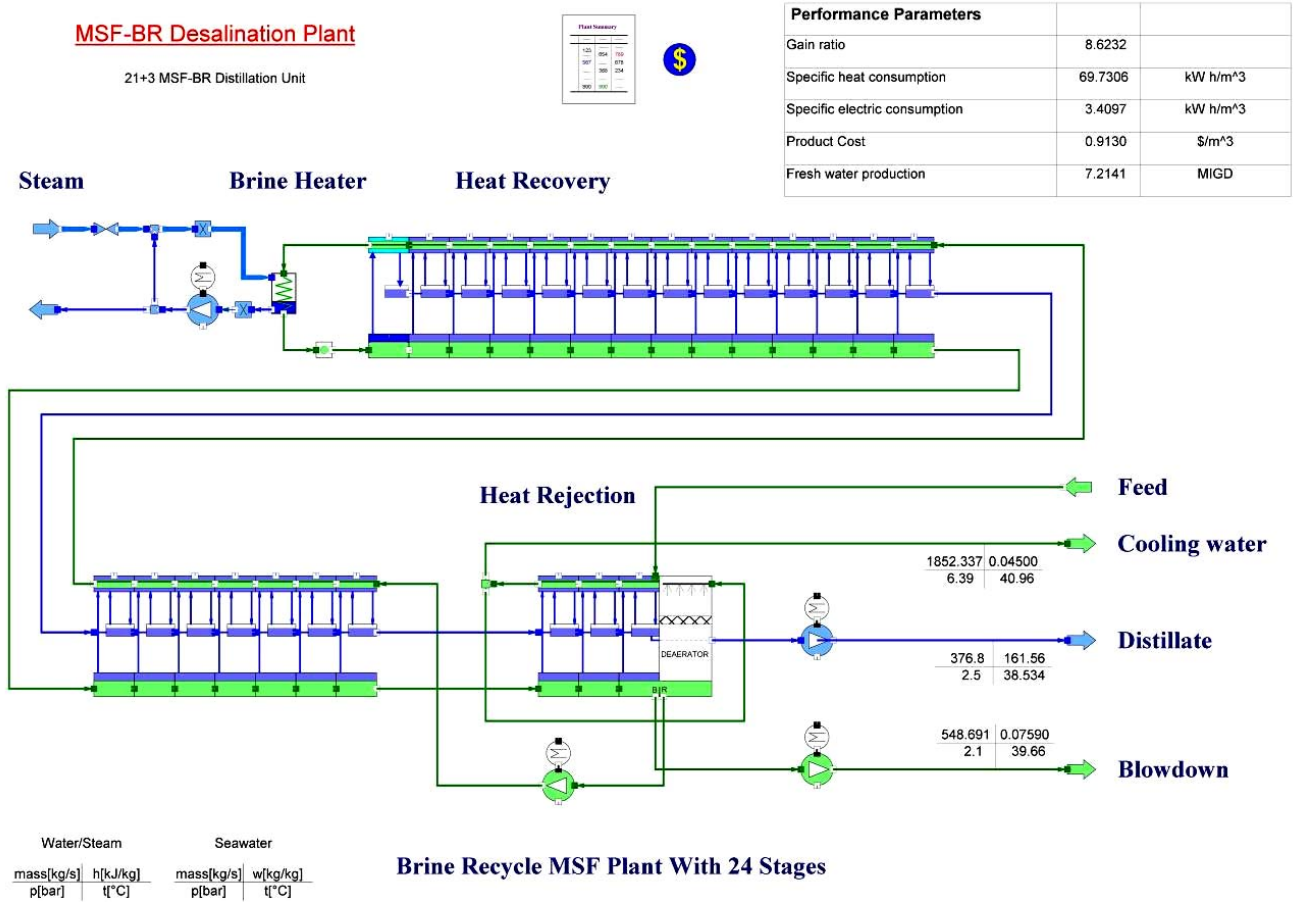


Fig. 5b. Flow sheet of MSF-BR system (IPSEpro® software).

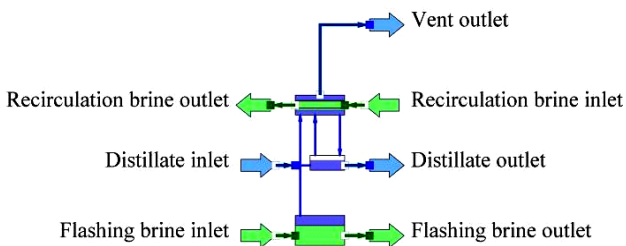


Fig. 6. Schematic diagram for the flashing stage (IPSEpro® software).

condensable gases (4%) in each plant section. The fouling resistances were assumed to be 0.000263, 0.00014915 and 0.0001757 m<sup>2</sup>°C/W in the brine heater, heat recovery and heat rejection sections, respectively [13]. However, if accurate measurements for these parameters were available, the model can predict data with much more accuracy.

The amount of heat transferred from vapor to recirculation brine in each stage is shown in Fig. 12. The re-

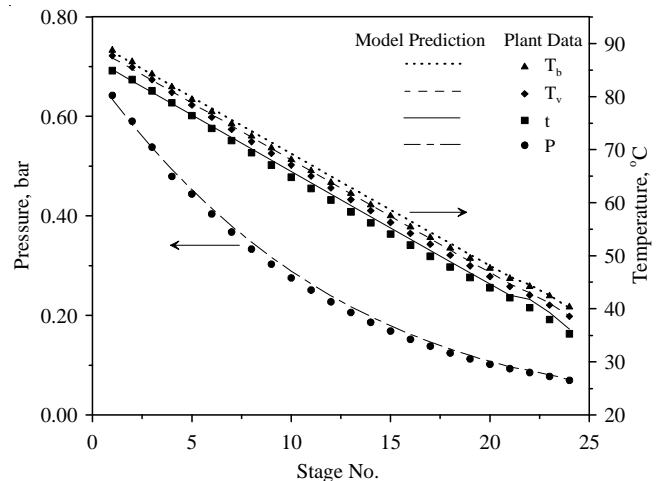


Fig. 7. Pressure and temperatures profiles (lines for model, symbol for plant actual data).

sults in Fig. 12 show that the predicted values of heat transfer from vapor to recirculation brine have similar decreasing trend as the predicted results of the overall

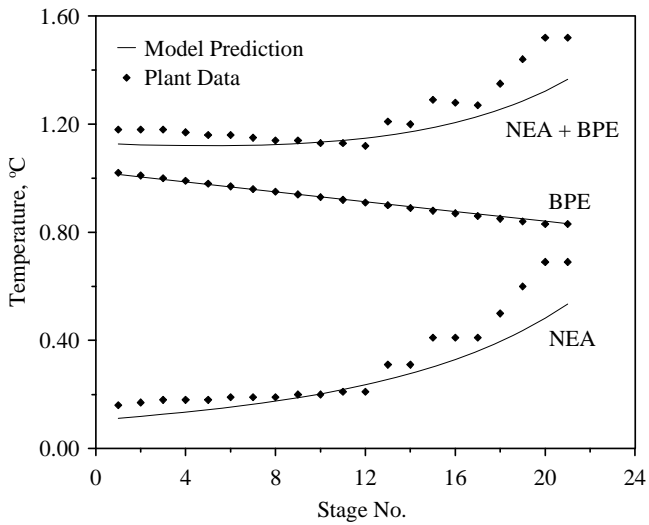


Fig. 8. Temperature loss profile.

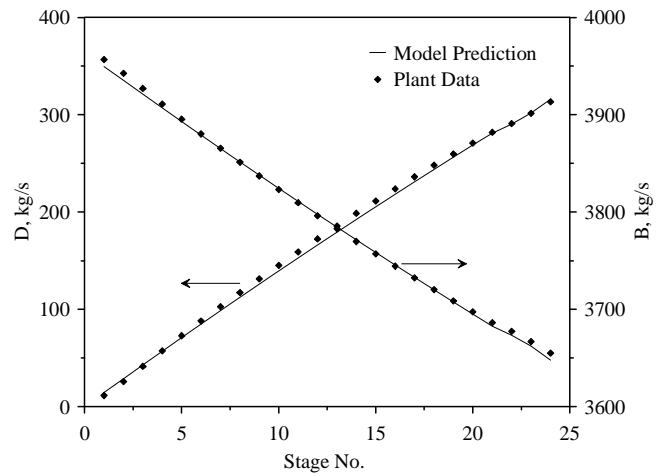


Fig. 9. Distillate and flashing brine flow rate at each stage.

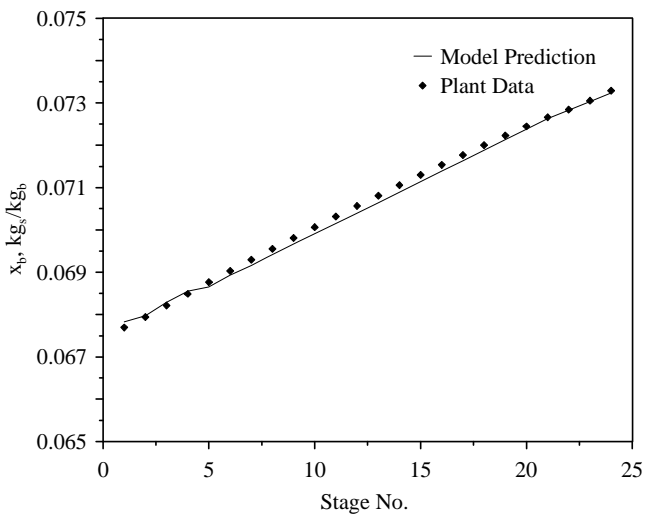


Fig. 10. Flashing brine salinity.

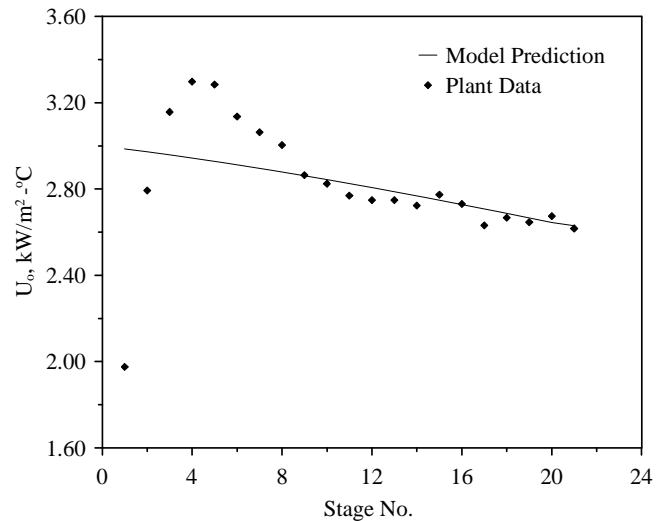


Fig. 11. Overall heat transfer coefficient profile.

heat transfer coefficient in Fig. 11. In Fig. 11, the difference between the overall heat transfer coefficient obtained by the model and the actual data for the first point is almost 50%. This difference causes a difference of only 25% in the heat transfer in Fig. 12, whereas for the heat rejection section in Fig. 11 the difference is very small, at the same time it causes a large difference in Fig. 12. It is valuable and worthwhile to perform a sensitivity analysis for each variable on others, which can be considered in future research work.

Fig. 13 illustrates the effect of the top brine temperature on the gain output ratio (GOR). The GOR of 8 is a common value among various MSF plants. However, systems operated at clean conditions can reach values close

to 10. As the operation period proceeds, fouling and scaling start to reduce the overall heat transfer coefficient, hence GOR decreases gradually. It is normal to allow the system to operate at GOR below 7, where full shutdown takes place and acid cleaning and in some events mechanical cleaning are necessary to restore the unit characteristics to the original design conditions [19]. As shown in Fig. 13, the GOR increases almost linearly with the increase of the TBT; operation at higher TBT increases the flashing range, hence increases the amount of distillate. The increase of the GOR reduces the specific thermal energy consumption as shown in Fig. 14.

Fig. 15 illustrates the effect of TBT on the specific flow rate of the cooling water (CW), feed (F) and recirculation

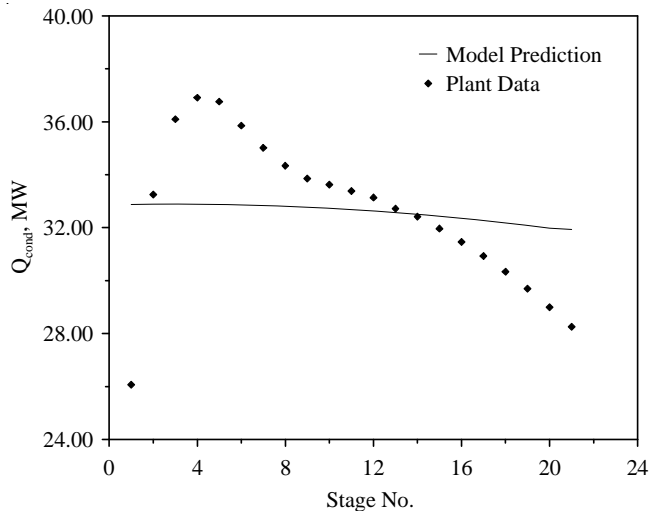


Fig. 12. Heat transferred from vapor to recirculation brine.

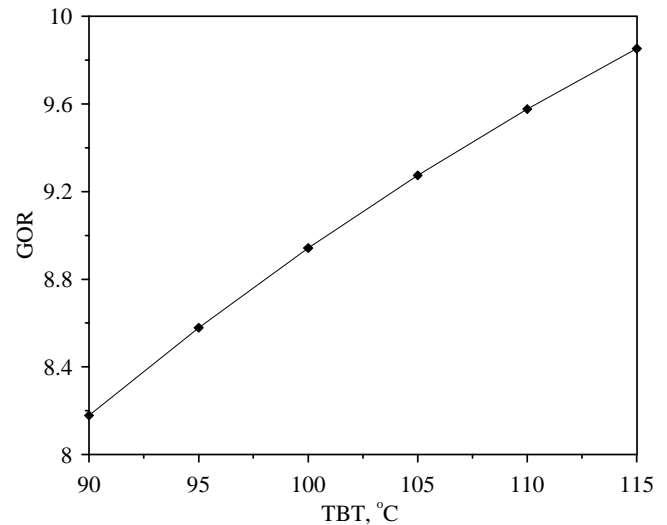


Fig. 13. Effect of top brine temperature on the plant gain output ratio.

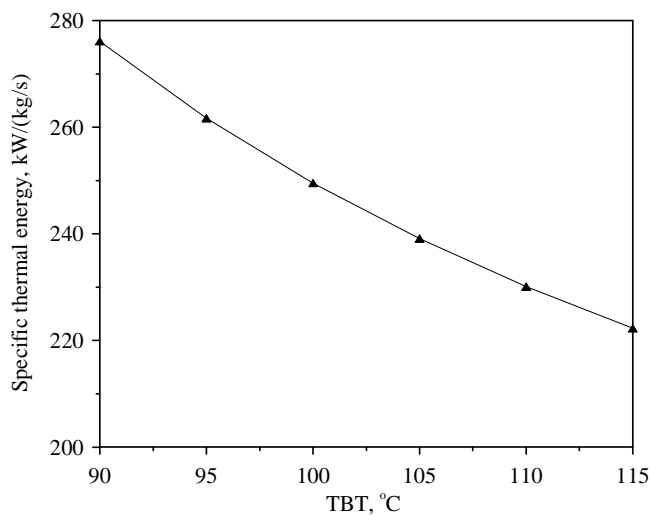


Fig. 14. Effect of top brine temperature on the specific thermal energy.

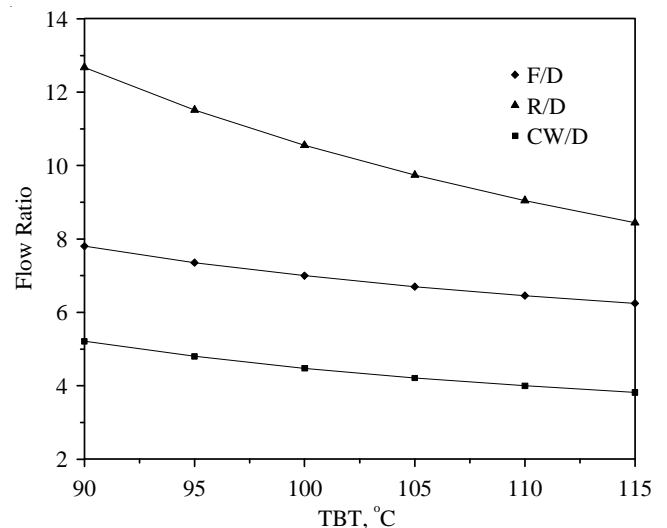


Fig. 15. Effect of top brine temperature on the specific flow rate of the cooling water, feed and recirculation brine.

brine (R) streams. The results show that as TBT increases the specific cooling water flow rate decreases. This is explained in the light of the results obtained in Fig. 13, where GOR increases at high values of TBT, which is a result of using less amount of heating steam to produce constant distillate rate. Reduction in the amount of heating steam tends to decrease the amount of energy added to the system, hence decrease the amount of energy removed via cooling seawater. The specific flow rate of feed and recirculation brine decreases with the increase of TBT for the same reasons, which leads to increasing the plant performance by reducing the power required for pumping these streams.

Fig. 16a shows the value of exergy destruction in kW for the three components of the flashing stage. As shown in the figure, the exergy destruction increases as TBT increases for the three components. It is known that the increase in the temperature difference during heat transfer process leads to the increase in the process irreversibility; hence this increases the value of exergy destruction. One should notice that the value of exergy destruction for each component represents the summation of exergy destructions of that component in all stages. It is clear that most exergy destruction occurred in the tube bundle was due to the high mass flow rate and temperature differences compared to the other two components,

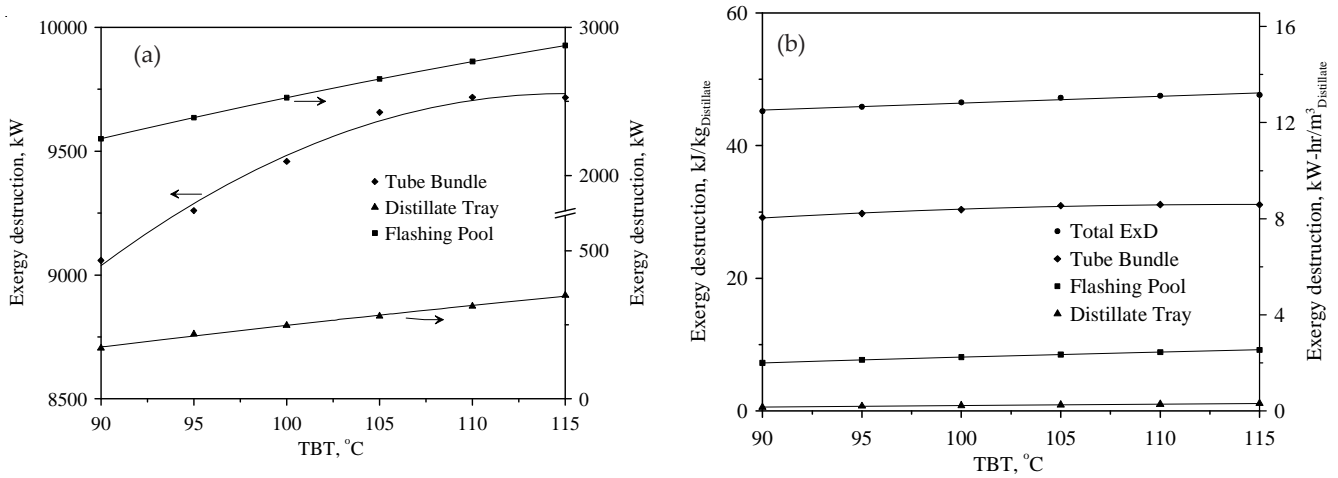


Fig. 16. Effect of top brine temperature on exergy destruction.

and the least is in the distillate tray due to small amount of distillate mass flow rate. Fig. 16b shows the exergy destruction of the three components per unit mass and volume of distillate product. The results also show the total exergy destruction in the MSF–BR plant including the brine heater section.

### 5. Conclusions

In this research, different approaches for MSF–BR modeling and simulation have been reviewed. The rigorous steady state model for the MSF–BR desalination system was presented. A parametric study was carried out in the light of the first and second law of thermodynamics. The computational results for the steady state MSF–BR model were verified against actual data at Azzour South desalination plant. The results show that:

1. The proposed mathematical model was able to predict the MSF–BR process performance with a very good agreement against actual data.
2. The calculation of the heat transfer coefficient plays an important role in the model and has a great effect on numerical results.
3. As the top brine temperature increases the specific thermal energy consumption decreases.
4. The top brine temperature affects the specific flow rate of various brine streams.
5. The exergy destruction increases as the top brine temperature increases for the three components of the flashing stage, where tube bundle is the highest and distillate tray is the lowest.

### Symbols

- $A$  — Heat transfer area,  $m^2$
- $A_{cross}$  — Tube cross section area,  $m^2$
- $A_{surface}$  — Heat transfer surface area of the tube,  $m^2$

- $C$  — Average specific heat of brine and distillate,  $kJ/kg\ ^\circ C$
- $Cd$  — Orifice discharge coefficient
- $Cp$  — Specific heat at constant pressure,  $kJ/kg\ ^\circ C$
- $CR$  — Concentration ratio
- $d_i$  — Inner tube diameter,  $m$
- $d_o$  — Outer tube diameter,  $m$
- $e$  — Stream specific exergy,  $kJ/kg$
- $Ex$  — Exergy,  $kW$
- $ExD$  — Exergy destruction,  $kW$
- $g$  — Gravitational acceleration,  $m/s^2$
- $h$  — Stream specific enthalpy,  $kJ/kg$
- $H_b$  — Brine height,  $m$
- $H_{gt}$  — Gate height,  $m$
- $h_i$  — Internal heat transfer coefficient,  $kW/m^2\ ^\circ C$
- $h_o$  — External heat transfer coefficient,  $kW/m^2\ ^\circ C$
- $k_b$  — Brine thermal conductivity,  $kw/m\ ^\circ C$
- $k_l$  — Liquid condensate thermal conductivity,  $kw/m\ ^\circ C$
- $k_{tube}$  — Tube material thermal conductivity,  $kw/m\ ^\circ C$
- $L_{stg}$  — Stage length,  $m$
- $LMTD$  — Logarithmic mean temperature difference,  $^\circ C$
- $L_{tube}$  — Tube length,  $m$
- $m$  — Mass flow rate,  $kg/s$
- $M_s$  — Salt molecular weight,  $kg/kmol$
- $M_w$  — Water molecular weight,  $kg/kmol$
- $n$  — Number of tubes in vertical direction in the tube bundle
- $N$  — Number of stages
- $NCG$  — Non-condensable gases
- $N_{tube}$  — Number of tubes in the tube bundle
- $P, p$  — Pressure,  $kPa$
- $P_e$  — Environment pressure,  $kPa$
- $Pr$  — Prandtle number
- $Q$  — Heat transfer,  $kW$
- $Re$  — Reynolds number

$R_{f,i}$	– Internal fouling resistance, $m^2 \text{ }^\circ\text{C}/\text{kW}$
$R_{f,o}$	– External fouling resistance, $m^2 \text{ }^\circ\text{C}/\text{kW}$
$\bar{R}_u$	– Universal gas constant, $\text{J}/\text{kmol}\cdot\text{K}$
$s$	– Stream specific entropy, $\text{kJ}/\text{kg }^\circ\text{C}$
$SL_{\text{Stg}}$	– Shell load of the stage, $\text{kg}/\text{s}\cdot\text{m}$
$T, t$	– Temperature, $^\circ\text{C}$
$T_b$	– Bulk temperature, $^\circ\text{C}$
$T_e$	– Environment temperature, $\text{K}$
$T_{\text{film}}$	– Condensate film temperature, $^\circ\text{C}$
$T_o$	– Top brine temperature, $^\circ\text{C}$
$T_{\text{wall}}$	– Tube wall temperature, $^\circ\text{C}$
$U_o$	– Overall heat transfer coefficient, $\text{kw}/\text{m}^2 \text{ }^\circ\text{C}$
$v$	– Stream specific volume, $\text{m}^3/\text{kg}$
$V_{\text{rel}}$	– Vapor release velocity, $\text{m}/\text{s}$
$V_b$	– Brine velocity, $\text{m}/\text{s}$
$w$	– Stream salinity, $\text{kg}_{\text{salt}}/\text{kg}_{\text{water}}$
$W_{\text{Stg}}$	– Stage width, $\text{m}$
$y$	– Brine salt mole fraction
$y_o$	– Seawater salt mole fraction at $w_e$

#### Greek

$\eta_{\text{BH}}$	– Brine heater thermal efficiency
$\eta_{\text{evap}}$	– Evaporator thermal efficiency
$\eta_{\text{FP}}$	– Flashing pool thermal efficiency
$\eta_{\text{II}}$	– Second law (exergetic) efficiency
$\eta_{\text{TB}}$	– Tube bundle thermal efficiency
$\lambda_s$	– Steam latent heat, $\text{kJ}/\text{kg}$
$\lambda_v$	– Vapor latent heat, $\text{kJ}/\text{kg}$
$\mu_b$	– Brine viscosity, $\text{kg}/\text{m s}$
$\mu_{b,w}$	– Brine viscosity at wall temperature, $\text{kg}/\text{m s}$
$\rho$	– Density, $\text{kg}/\text{m}^3$
$\delta T$	– Temperature difference

#### Subscripts

B_in	– Brine inlet
B_out	– Brine outlet
bh	– Brine heater
B <sub>l</sub>	– Blow down
BPE	– Boiling point elevation
C	– Condensate
ch	– Chemical
cw	– Cooling water
D	– Distillate
dem	– Demister
D_in	– Distillate in
D_out	– Distillate out
DT	– Distillate tray
e	– Environment, or exit
F	– Feed
FDV	– Flashed distillate vapor
FBV	– Flashed brine vapor
FP	– Flashing pool
i	– Inner, or inlet, or stage number
l	– Liquid

M	– Make up
NEA	– Non-equilibrium allowance
o	– Outer
R_in	– Recycle brine in
R_out	– Recycle brine out
rc	– Recycle brine
s	– Salt
S	– Steam
TB	– Tube bundle
th	– Thermal
v	– Vapor
w	– Water

#### Abbreviations

BPE	– Boiling point elevation
FBV	– Flashed brine vapor
FDV	– Flashed distillate vapor
GOR	– Gain output ratio
LMTD	– Logarithmic mean temperature difference
MIGD	– Million imperial gallon per day
MSF	– Multistage flashing
MSF–BR	– Multistage flashing with brine recirculation
MSF–OT	– Once through multistage flashing
NEA	– Non-equilibrium allowance
TBT	– Top brine temperature
TDM	– Tri-diagonal matrix
TDS	– Total dissolved salts

#### References

- [1] M.A. Soliman, A mathematical model for MSF multi-stage flash desalination plants, *J. Eng. Sci. Univ. Riyadh*, 7(2) (1981) 143–150.
- [2] W.L. Griffin and R.M. Keller, Saline, A FORTRAN Computer Program for Process Design of Saline Water Conversion Plant Using Multi-Stage Flash Evaporation Process, Oak Ridge National Laboratory, ORNL-TM-1299 report, 1965.
- [3] A.M. Helal, Upgrading of Umm Al-Nar East 4-6 MSF desalination plants, *Desalination*, 159 (2003) 43–60.
- [4] E.E. Tarifa and N.J. Scenna, A dynamic simulator for MSF plants, *Desalination*, 138 (2001) 349–364.
- [5] A.S. Hanafi and M.S. Shousha, Dynamic modeling of MSF desalination plants: I. Governing equations, *Proc. IDA World Congress, Bahamas, 2003*, pp. 1–31.
- [6] A. Gambier and E. Badreddin, Dynamic modeling of MSF plants for automatic control and simulation purposes: A survey, *Desalination*, 166 (2004) 191–204.
- [7] A.M. Helal, A.M. El-Nashar, E. Al-Katheeri and S. Al-Malek, Optimal design of hybrid RO/MSF desalination plants. Part I: Modeling and algorithms, *Desalination*, 154 (2003) 43–66.
- [8] A.M. Helal, M.S. Medani, M.A. Soliman and J.R. Flower, A tridiagonal matrix model for multistage flash desalination plants, *Computers Chem. Eng.*, 10(4) (1986) 327–342.
- [9] I.S. Al-Mutaz and M.A. Soliman, Simulation of MSF desalination plants, *Desalination*, 74 (1989) 317–326.
- [10] A. Husain, A. Hassan, D.M. Al-Gobaisi, A. Al-Radif, A. Woldai and C. Sommariva, Modeling, simulation, optimization and control of multistage flashing (MSF) desalination plants. Part I: Modeling and simulation, *Desalination*, 92 (1993) 21–41.
- [11] S.E. Aly and K. Fathalah, MSF – a mathematical model, *Proc. IDA World Congress, Abu Dhabi, 1995*, pp. 203–226.

- [12] H.T. El-Dessouky, H.I. Shaban and H. Al-Ramadan, Steady-state analysis of multi-stage flash desalination process, *Desalination*, 103 (1995) 271–287.
- [13] H.T. El-Dessouky and S. Bingulac, A stage-by-stage algorithm for solving the steady state model of multi-stage flash desalination plants, *Proc. IDA World Congress*, Abu Dhabi, 1995, pp. 251–277.
- [14] H.T. El-Dessouky and S. Bingulac, Solving equations simulating the steady-state behavior of the multi-stage flash desalination process, *Desalination*, 107 (1996) 171–193.
- [15] P.J. Tomas, S. Bhattacharyya, A. Patra and G.P. Rao, Steady state and dynamic simulation of multi-stage flash desalination plants: A case study, *Computers Chem. Eng.*, 22 (10) (1998) 1515–1529.
- [16] N.H. Aly and A.K. El-Fiqi, Thermal performance of seawater desalination systems, *Desalination*, 158 (2003) 127–142.
- [17] M.G. Marcovecchio, S.F. Mussati, P.A. Aguirre and N.J. Scenna, Optimization of hybrid desalination processes including multi stage flash and reverse osmosis systems, *Desalination*, 182 (2005) 107–118.
- [18] A. Husain, K. Wangnick and A. Radif, Case study on planning a large scale multistage flash desalination plant in thermal desalination processes, *Encyclopedia of Desalination and Water Resources*, Oxford, UK, 2004, <http://www.desware.net>.
- [19] H.T. El-Dessouky and H.M. Ettouney, *Fundamentals of Salt Water Desalination*, Elsevier Science, 2002.
- [20] F. Incropera, D. Dewitt, T. Bergman and A. Lavine, *Fundamentals of Heat and Mass Transfer*, 6th ed., Wiley, 2007..
- [21] A.J. Chapman, *Fundamentals of Heat Transfer*, Macmillan, 1987.
- [22] H.T. El-Dessouky, H.M. Ettouney and Y. Al-Roumi, Multi-stage Flash desalination: present and future outlook, *Chem. Eng. J.*, 73 (1999) 173–190.
- [23] S. Henning, K. Wangnick and K. Wangnick, Comparison of different equations for the calculation of heat transfer coefficients in MSF multi-stage flash evaporators, *Proc. IDA World Congress*, Abu Dhabi, 1995, pp. 515–524.
- [24] SimTech Simulation Technology, *IPSE pro – PSE User Manuals*, Ver. 4.0, Build 869, 2004.
- [25] H.K. Abdulrahim, Multi-objective optimization of MSF-RO and MSF-MVC hybrid desalination systems, Ph.D. thesis, Cairo University, Egypt, 2006.

## Appendix A

### Boiling point elevation [19]

$$T_{BPE} = A_0 \cdot TDS + A_1 \cdot TFS^2 + A_2 \cdot TDS^3 \quad (A1)$$

where

$$A_0 = a_0 + b_0 \cdot T + c_0 \cdot T^2$$

$$A_1 = a_1 + b_1 \cdot T + c_1 \cdot T^2$$

$$A_2 = a_2 + b_2 \cdot T + c_2 \cdot T^2$$

and

$$a_0 = 82543.1 \cdot 10^{-6} \quad b_0 = 188.3 \cdot 10^{-6} \quad c_0 = 2.02 \cdot 10^{-6}$$

$$a_1 = -762.5 \cdot 10^{-6} \quad b_1 = 9.02 \cdot 10^{-6} \quad c_1 = -0.52 \cdot 10^{-6}$$

$$a_2 = 152.2 \cdot 10^{-6} \quad b_2 = -3.0 \cdot 10^{-6} \quad c_2 = 0.03 \cdot 10^{-6}$$

### Non-equilibrium allowance

The non-equilibrium allowance ( $T_{NEA}$ ) is an irreversible phenomenon that characterizes the flashing process in the stage, it leads to an increase in the brine temperature in the flashing pool with respect to the ideal equilibrium conditions. The non-equilibrium allowance temperature can be estimated using the following equation [19].

$$T_{NEA} = \alpha \left( \frac{NEA_{10}}{\alpha} \right)^{(0.3281L_{Stg})} \quad (A2)$$

where

$$NEA_{10} = (0.9784^{f_{B,out}}) (15.7378^{H_b}) (1.3777^{SL_{Stg} \cdot 10^{-6}})$$

$$\alpha = 0.5 \Delta T + NEA_{10}$$

### Shell load

Shell load is defined as brine flow rate per unit width of the stage:

$$SL_{Stg} = \frac{m_{B,in}}{W_{Stg}} \quad (A3)$$

### Brine pool height

The brine pool height is estimated using the following equation [19]

$$H_{gt} = \frac{m_{B,in}}{CdW_{Stg}} \left( \frac{2 \cdot 10^5 \Delta P}{v_{B,out}} \right)^{(-0.5)} \quad (A4)$$

$\Delta P$  is the pressure drop across the stage and  $W_{Stg}$  is the stage width which taken the same as the weir width and  $Cd$  is the discharge coefficient of the weir, equal to 0.6 in the present work.

### Demister pressure drop

The pressure drop in the demister can be calculated using the following equations [18]

$$\Delta P_{dem} = 0.012 \cdot 10^{-5} \cdot e^{\Phi}$$

$$\Phi = 10.51 - 1.287 \cdot \log C + 0.3784 (\log C)^2 \frac{3.281 \cdot V_{rel}}{\sqrt{\frac{\rho_1 - \rho_v}{\rho_1} - 0.075}} \quad (A5)$$

$$C = 737.3 \cdot FBV \cdot \rho_1 \cdot V_{rel}$$

$$V_{rel} = 0.078 \cdot \sqrt{\frac{\rho_1 - \rho_v}{\rho_v}}$$

The temperature drop due to pressure drop through the demister can be evaluated using the saturated steam properties. Temperature drop caused by pressure drop over the tube bundle is evaluated from the following correlation [18]

$$\Delta T_{TB} = 0.236 - 0.0012 \cdot t_C \quad (A6)$$

The flashed brine vapor pressure can be calculated using the following equation assuming saturated vapor.

$$p_{FBV} = P_{\text{sat}}(t_{FBV}) \quad (A7)$$

Since the flashing process is not under equilibrium, the pressure of the flashed vapor is equal to the partial pressure of the vapor in the seawater solution, and it is less than the brine pressure.

## Appendix B

### Stream models and properties

#### Seawater stream model

Seawater stream model is a set of thermo-physical properties equations and functions used to calculate the entire stream properties set by knowing any independent properties beside the mass and the salt concentrations.

#### Thermo-physical properties of seawater and brine

##### Density of the brine [19]

$$\rho_b = A_0 + A_1 t + A_2 t^2 + A_3 t^3 \quad (B1)$$

$$A_0 = 1002.4 + 754.8 w_b + 236.3 w_b^2$$

$$A_1 = -0.1338 - 0.935 w_b - 0.0976 w_b^2$$

$$A_2 = -0.3375 \cdot 10^{-2} + 0.996 \cdot 10^{-2} w_b - 0.0439 w_b^2$$

$$A_3 = 0.313 \cdot 10^{-5} - 0.163 \cdot 10^{-4} w_b + 0.244 \cdot 10^{-3} w_b^2$$

##### Specific volume of the brine

$$v_b = 1/\rho_b(t, w_b) \quad (B2)$$

##### Specific enthalpy of the brine [19]

$$h_b = A_0 + 10^{-3} (A_1 t + A_2 t^2 + A_3 t^3 + A_4 t^4) \quad (B3)$$

$$A_0 = 9.62964 w_b - 431.2404 w_b^2$$

$$A_1 = 1.000000433 (4206.8 - 6619.7 w_b + 12288 w_b^2)$$

$$A_2 = 0.5000002164 (-1.1262 + 54.178 w_b - 227.19 w_b^2)$$

$$A_3 = 0.3333334776 (0.0120264 - 0.53566 w_b + 1.8906 w_b^2)$$

$$A_4 = 0.2500001082 (0.68774 \cdot 10^{-6} + 0.1517 \cdot 10^{-2} w_b - 0.4268 \cdot 10^{-2} w_b^2)$$

##### Specific heat of the brine [19]

$$C_p = 10^{-3} (A_0 + A_1 t + A_2 t^2 + A_3 t^3) \quad (B4)$$

$$A_0 = 4206.8 - 6619.6 w_b + 12288.0 w_b^2$$

$$A_1 = -1.1262 + 54.1785 w_b - 227.19 w_b^2$$

$$A_2 = -0.0112026 - 0.53566 w_b + 1.8906 w_b^2$$

$$A_3 = 0.68774 \cdot 10^{-6} + 0.1517 \cdot 10^{-2} w_b - 0.44268 \cdot 10^{-2} w_b^2$$

##### Specific entropy of the brine

$$s_b = C_p \cdot \ln\left(\frac{t + 273.15}{273.15}\right) \quad (B5)$$

The entropy of the seawater is assumed zero at temperature equal 0°C. The effect of salinity on entropy will be implicitly included through the specific heat,  $C_p$ .

##### Specific exergy of the brine

The following environmental conditions are used to calculate the stream exergy:

$$T_e = 298.15 \text{ K}$$

$$P_e = 1.013 \text{ bar}$$

$$w_e = 0.045 \text{ kg}_{\text{salt}}/\text{kg}_{\text{water}} \quad (B6)$$

However, the environmental temperature in °C is  $t_0$ , where  $t_0 = T_e - 273.15$  was used in some equations. The total specific exergy of the seawater stream is the summation of thermal, chemical and physical exergies. Thermal exergy is due to the temperature, chemical exergy is due to the salt concentration while physical exergy is due to the pressure.

$$e = e_{\text{th}} + e_{\text{ch}} + e_p \quad (B7)$$

##### Thermal exergy

The specific thermal exergy of seawater stream can be calculated using Eq. (B8)

$$e_{\text{th}} = (h - h_0) - T_e (s - s_0) \quad (B8)$$

##### Chemical exergy

The specific chemical exergy of the seawater stream is due to salt concentration and can be calculated using

the following equation [25]

$$e_{ch} = \frac{\bar{R}_u \cdot T_e \cdot \ln\left(\frac{y}{y_0}\right)}{M_w} \quad (B9)$$

In Eq. (B9), the mole fractions  $y$  and  $y_0$  are calculated as follows.

Number of moles of water in the solution is ( $n_w$ ) and can be calculated by

$$\begin{aligned} n_w &= \frac{c_w}{M_w} \\ c_w &= 1 - w_b \end{aligned} \quad (B10)$$

where  $c_w$  is the pure water concentration in the seawater solution, and  $M_w$  is the molecular weight of pure water = 18.0 kg/kmol. Number of moles of salt in the solution,  $n_s$ , can be calculated using the following equation.

$$n_s = \frac{w_b}{M_s} \quad (B11)$$

where the average molecular weight of the TDS in typical seawater is  $M_s = 31.4$  kg/kmol. The mole fraction of pure water in the seawater solution can be calculated as follows

$$y = \frac{n_w}{n_w + n_s} \quad (B12)$$

$y_0$  can be calculated using same procedure after changing  $w_b$  into  $w_e$ .

It is very interesting to note that the chemical exergy of the brine could be positive or negative. For seawater with concentration equal to the environment concentration ( $w_e$ ), the chemical exergy will be zero; however, if the seawater concentration increased above  $w_e$ , its chemical exergy will be negative value. This fact can be simply explained. For brine with concentration higher than the environment concentration, one should pay an exergy to separate the extra salt from the brine to reduce its concentration to the environment concentration; paid exergy means negative exergy for the brine stream. In the low temperature side of the desalination plant, when the thermal exergy value is small, the total specific exergy could be zero or even negative depending on the brine concentration. Following the same logic, the chemical exergy of the pure water will be always positive.

*Pressure exergy*

The exergy of the flow due to the pressure can be estimated using [25].

$$e_p = 100(P - P_e)v_0 \quad (B13)$$

**Appendix C**

*Azzour desalination plant data*

Table 1C  
Evaporators

	Recovery			Rejection
Stage No.	1–4	5–12	13–21	22–24
No. of stages	21			3
Heat transfer area	77,206 m <sup>2</sup>			9,444 m <sup>2</sup>
No. of tubes/stage	1451			1588
Tube size	43.8 mm OD × SWG. 18 ave 41.4 mm ID			34.2 mm OD × SWG. 18 ave. 31.8 mm ID
Design temperature				
Shell side	115	97	73	50
Tube side	110	92	68	45
Design pressure				
Shell side	1.0 kg/cm <sup>2</sup> g and full vac.			1.0 kg/cm <sup>2</sup> g and full vac.
Tube side, water box	3.43		5.85	3.96
Tube side, tube plate	5.15		8.78	4.95
Dimension	8.340 m (height) × 17.660 m (width) × 3.998 m (length)			
Weight				
Empty, operation, flooded	2,360 ton, 4,600 ton, 7,190 ton			

Table 2C  
Brine heater

No. of passes	1
Fluids	
Shell side	heating steam
Tube side	recycle brine
Design temperature	
Shell side	155.47°C
Tube side	115°C
Design pressure	
Shell side	4.575 kg/cm <sup>2</sup> G
Tube side	1.632 kg/cm <sup>2</sup> G
No. of tubes	1367
Heat transfer area	3544 m <sup>2</sup>
Tube pitch	55 mm, triangular
Tube size	
O.D.	43.8 mm
I.D.	41.36 mm
Length	18991 mm
Shell dimension	
I.D.	2.800 m
Length	23.956 m
Weight	
Empty, operation, flooded	100 ton, 160 ton, 213 ton

Table 3C  
Operating conditions

Item	Value (t/h)	Temperature (°C)
SW to rejection section	9,629.3	32.22
Makeup	2,925.4	40.23
Brine blow down	499.36	40.50
R. brine from brine heater	14,286.0	90.56
Distillate	1,127.7	38.60
Steam to brine heater	140.96	100.00
GOR	8.0	